Bull. Mater. Sci. (2020) 43:158
https://doi.org/10.1007/s12034-020-02137-z

Photoinduced synthesis of variable-sized magnetite nanoparticles and their photodegradation for orange II

BO LIU[1,#], NANNAN WANG[1,#], JIAYING JIN[1,#], HUI LIU[1] and RUFEN CHEN[1,2,*]

[1]College of Chemistry and Material Science, Hebei Normal University, Shijiazhuang 050024, People's Republic of China
[2]National Demonstration Center for Experimental Chemistry, Hebei Normal University, Shijiazhuang 050024, People's Republic of China
[*]Author for correspondence (chenrufen@mail.hebtu.edu.cn)
[#]These authors contributed equally to this study.

MS received 24 May 2019; accepted 9 May 2020; published online 1 July 2020

Abstract. Magnetite (Fe_3O_4) nanoparticles with different particle sizes (9.9–29.1 nm) were prepared by using the aerial oxidation method under light irradiation with various wavelengths at room temperature. The photocatalytic degradation of orange II using Fe_3O_4 nanoparticles as photocatalysts was evaluated. Experimental results showed that the particle sizes of Fe_3O_4 nanocrystals decreased gradually with the decreasing wavelengths of light irradiation. With the decrease in the size of the samples, the Fe_3O_4 nanoparticles exhibited a large surface area and high adsorption. Furthermore, the small-particle-sized Fe_3O_4 sample could cause an appropriate red shift of the spectra and promote the decomposition of H_2O_2, and produce high-content $^{\bullet}OH$ radicals, which lead to an improvement of photodegradation efficiency of orange II.

Keywords. Fe_3O_4; particle size; light irradiation; photodegradation.

1. Introduction

Azo dyes are highly recalcitrant environmental pollutants [1]. Among these azo dyes, orange II accounts for >50% of the world production of dyes used in the textile-manufacturing industry [2]. Therefore, effective wastewater treatment methods are necessary. In recent years, advanced oxidation processes (AOPs) have become increasingly important in the removal of dyes from aqueous solutions because they can reach total mineralization [3]. Among the AOPs, a lot of attention has been focused on the use of heterogeneous photocatalysis to oxidize dyes [4]. A recent study suggested that Fe II-bearing minerals, such as magnetite (Fe_3O_4), have become more effective catalysts for heterogeneous catalytic oxidation of organic pollutants compared with Fe III oxides [5–7]. In addition, it was found that Fe_3O_4 is an efficient catalyst for Fenton-like processes [8–14] owing to the content of Fe^{2+} that might play an indispensable role in initiating the Fenton reaction. Fe_3O_4 also demonstrated peroxidase-like activity, which enables H_2O_2 activation [15].

The properties of Fe_3O_4 depend on their particle size [16–20], and small-sized nanoparticles present higher chemical activities [17–19]. Small-sized Fe_3O_4 nanoparticles have been prepared by various methods such as laser ablation, micro-emulsions, high-temperature decomposition of organic precursors, etc. [20]. However, smaller (<20.0 nm) monodispersed Fe_3O_4 nanoparticles without surface modification in aqueous solutions at room temperature only have limited success. Previous studies have revealed that an oxidation reaction was accelerated by visible light in the presence of ethylenediaminetetraacetic acid (EDTA). A rapid oxidation rate was favourable for decreasing the sizes of the Fe_3O_4 nanoparticles in aqueous systems [21]. But, visible light sources with high power release large amounts of heat, thereby increasing the temperature of reaction and waste energy. To our knowledge, the influence of light sources with different wavelengths on the synthesis of variable-sized Fe_3O_4 nanoparticles has not been reported yet.

In the present study, we report the preparation of variable-sized Fe_3O_4 nanoparticles by using the aerial oxidation method under light-emitting diode (LED) irradiation with different wavelengths at 20°C. The photocatalytic activity of nano-Fe_3O_4 with different particle sizes under visible light irradiation is also investigated.

2. Experimental

2.1 *Materials*

Ferrous sulphate ($FeSO_4 \cdot 7H_2O$), EDTA, hydroxylamine, 1,10-phenanthroline, sodium hydroxide (NaOH), sulphuric

Electronic supplementary material: The online version of this article (https://doi.org/10.1007/s12034-020-02137-z) contains supplementary material, which is available to authorized users.

acid (H_2SO_4), 30 wt% hydrogen peroxide (H_2O_2), *p*-benzoquinone (BZQ), disodium ethylenediaminetetraacetate (Na_2-EDTA), *tert*-butanol and orange II were obtained from Tianjin Chemical Reagent Company. Distilled water was used throughout this study.

2.2 *Synthesis of Fe_3O_4 nanoparticles*

An appropriate amount of $FeSO_4$ (0.5 M) and EDTA (0.2 M) were mixed under vigorous stirring. The pH of the mixture was controlled at 11.5 by adding a certain volume of NaOH solution (1.0 M). Subsequently, air (flow rate: 0.273 $m^3\ h^{-1}$) was passed through the suspension at 20 ± 1°C. Irradiation was performed at 625, 525, 470 and 425 nm wavelengths by using 50 W monowavelength LED lamps. The LED lamps at 625, 525, 470 and 425 nm mainly emitted red, green, blue and purple lights, respectively. Intensity of light (E) was detected using a light meter (TES-1336A). The Fe(II) concentration was determined by spectrophotometry [22,23]. The products were collected, washed with distilled water and then dried in air at 500°C for 18 h. The as-prepared samples under monowavelength light irradiation at 625, 525, 470 and 425 nm were denoted M-625, M-525, M-470 and M-425, correspondingly.

2.3 *Adsorption experiments*

The Fe_3O_4 (0.2 g) was added to 200 ml of orange II solution with varying concentrations in polyethylene centrifuge tubes. The mixture was agitated for 12 h in a thermostatic shaker bath under N_2 at 20 ± 1°C. Samples were centrifuged for 30 min to separate the solid catalyst from aqueous solution. Then the supernatants were analysed by using a UV–Vis spectrometer (SP-752, Shanghai) at a wavelength of 486 nm, and the adsorption capacity was calculated using equation (1) [24]:

$$\frac{C_e}{\Gamma} = \frac{1}{\Gamma_{max}} C_e + \frac{1}{K_\alpha \Gamma_{max}}, \tag{1}$$

where K_α is the adsorption equilibrium constant in l mol^{-1}, C_e is the equilibrium concentration in the solution in mol l^{-1} and Γ_{max} is the saturated adsorption capacity in mol g^{-1}.

2.4 *Measurement of photocatalytic activity*

Irradiation experiments were performed using a 100 W incandescent lamp. The 0.2 g solid catalyst was added to 200 ml of 1.0 mM orange II solution. The pH of the mixture was controlled at 3 by adding a certain volume of NaOH and $HClO_4$ solutions. The reaction system was magnetically stirred for 1.5 h in the dark to achieve adsorption equilibrium. Then, H_2O_2 was added into the reaction vessel and at the same time the lamp was switched on. The temperature of the reaction was maintained at 20°C. The samples were taken out after desired irradiation time intervals and filtered with a 0.22 μm Millipore filter to remove the catalyst. The concentration of orange II was evaluated using a UV–Vis spectrometer. The degradation efficiency (DE) of orange II was calculated by the method described in ref. [25].

2.5 *Sample characterization*

The structures of the catalyst were verified by X-ray diffraction (XRD) using a D8 Advance diffractometer with Kα radiation ($\lambda = 0.15418$ nm). The images of the catalyst were analysed by transmission electron microscopy (TEM) with a Hitachi H-7500 transmission electron microscope. UV–Vis diffuse reflectance spectra were recorded by using a Hitachi UV-3010 spectrophotometer with an integrating sphere. Specific surface areas (SSA) and total pore volumes (TPV) were analysed by nitrogen adsorption in a NOVA4000e nitrogen adsorption apparatus. The total iron concentration in solution was determined after reducing Fe(III) ions to Fe(II) ions with hydroxylamine, and then Fe(II) concentration was determined by spectrophotometry using 1,10-phenanthroline [22,23].

3. Results and discussion

3.1 *Preparation of Fe_3O_4 samples*

Figure 1 shows the XRD spectra of the as-prepared samples by using the aerial oxidation method under light irradiation with various wavelengths. All the diffraction peaks for each sample are well indexed to the standard diffraction peaks of magnetite with a cubic spinel structure (JCPDS 19-629) [21,26] (figure 1). Fourier-transform infrared spectra were examined (shown in supporting information figure S1), and the bands at 576.62–580.01 cm^{-1} can be attributed to the stretching vibration of the Fe–O bonds of Fe_3O_4 [27,28]. As shown in figure 1, crystallization of samples decreases gradually with the decreasing wavelength of light irradiation. The M-425 sample (figure 1d) demonstrates the weakest crystallization. The crystal sizes of samples were determined from the XRD pattern by using Scherrer's equation. The particle sizes of M-625, M-525, M-470 and M-425 are calculated to be 29.1, 23.2, 15.1 and 9.9 nm, respectively. Furthermore, the TEM images of the four Fe_3O_4 samples display a spherical shape (figure 2). The average particle sizes of the samples using TEM images are basically the same as calculated by the XRD data. These results indicate that the particle sizes of the Fe_3O_4 nanocrystals decrease gradually with the decreasing wavelength of light irradiation.

The difference in oxidation rates in the reaction systems may exert a profound impact on the particle size of the product. In the reaction system, the Fe(II) concentration decreases rapidly with the decreasing wavelength of light irradiation (figure 3). This observation indicates that the oxidation rate accelerates with the decreasing wavelength of light irradiation in the presence of EDTA. The fastest reaction rate is exhibited in the purple LED-lamp system (figure 3d). During the oxidation process, EDTA is chelated with Fe(II),

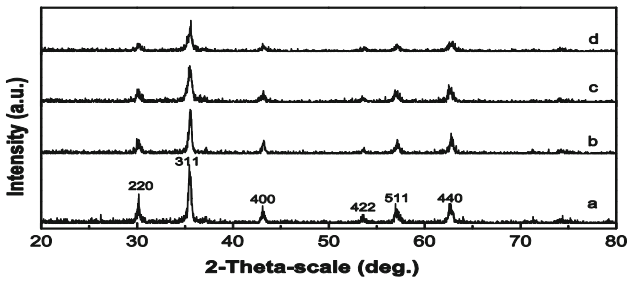

Figure 1. XRD patterns of the as-prepared samples under light irradiation with various wavelengths: (a) M-625, (b) M-525, (c) M-470 and (d) M-425.

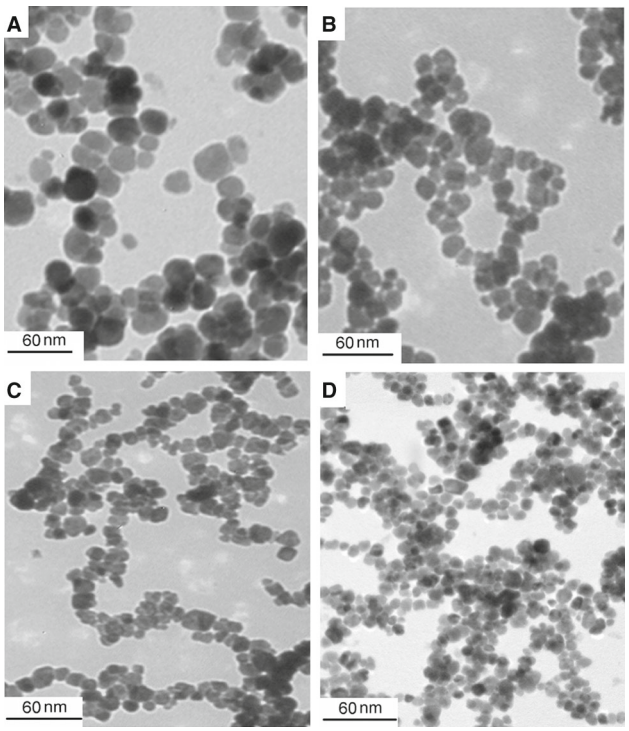

Figure 2. TEM images of the Fe_3O_4 samples under light irradiation with various wavelengths: (**A**) M-625, (**B**) M-525, (**C**) M-470 and (**D**) M-425.

thus forming Fe(II)–EDTA complexes, which exhibit strong ligand-to-metal charge absorption bands in the visible and near-UV regions [21]. Fe(II)–EDTA complexes have strong absorption towards purple light, and the purple light presents higher energy than other lights; hence, the oxidation rate is enhanced in the purple light system. A rapid oxidation rate is consequently favourable for the formation of small-particle-sized Fe_3O_4. Thus, the particle size of the M-425 sample obtained under purple light irradiation is the smallest.

3.2 *Surface area and adsorption of the Fe_3O_4 samples*

The adsorption isotherms of orange II on the M-625, M-525, M-470 and M-425 samples are shown in figure 4(B). These

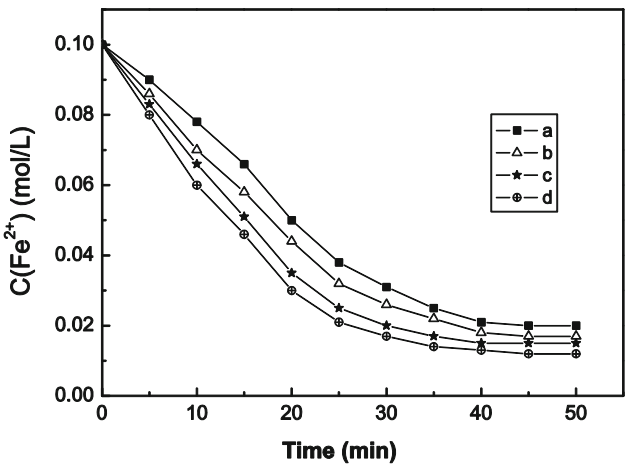

Figure 3. Changes of the Fe(II) concentration *vs*. reaction time under light irradiation with different wavelengths: (a) 625 nm, (b) 525 nm, (c) 470 nm and (d) 425 nm.

isotherms are well fitted by the Langmuir adsorption model, as shown in equation (1). The saturated adsorption amount (Γ_{max}) and adsorption equilibrium constant (K_α) of orange II on variable-sized Fe_3O_4 particles are listed in table 1. The Γ_{max} and K_α values of different Fe_3O_4 samples are ranked in the following order: M-625 < M-525 < M-470 < M-425. Obviously, both Γ_{max} and K_α increase with the decrease in the size of the Fe_3O_4 samples. The results imply that the small-particle-sized Fe_3O_4 samples demonstrate high-adsorption ability.

3.3 *Photodegradation of orange II*

The catalytic activity of M-425 that brings about degradation of orange II was investigated. Figure 5 outlines the effect of H_2O_2 concentration under visible light irradiation at pH 3. Degradation of orange II strongly depends on H_2O_2 concentration. The DE of orange II increases rapidly from 22 to 82% at 5 h with the increase of H_2O_2 concentration from 0 to 2 mM. The increase in the DE of orange II is not obvious with further increase in the H_2O_2 concentration (>2 mM). The suitable concentration of H_2O_2 is selected as 2 mM in this study.

The DE of orange II in M-425 system under different conditions is shown in figure 6. In contrast to the dark conditions (figure 6b), visible light irradiation (in the presence of H_2O_2) obviously improves the DE of orange II (figure 6a). This observation indicates that the presence of visible light can increase the DE of orange II in the M-425/H_2O_2 system. These results suggest that the coexistence of Fe_3O_4, visible light and H_2O_2 provides the most effective conditions for degradation of orange II. Under the best degradation conditions, the effect of variable-sized Fe_3O_4 samples as photocatalysts on the DE of orange II was also analysed. Figure 7 shows that the DE of orange II gradually improves with the decrease in the size of the Fe_3O_4 samples. The M-425 sample

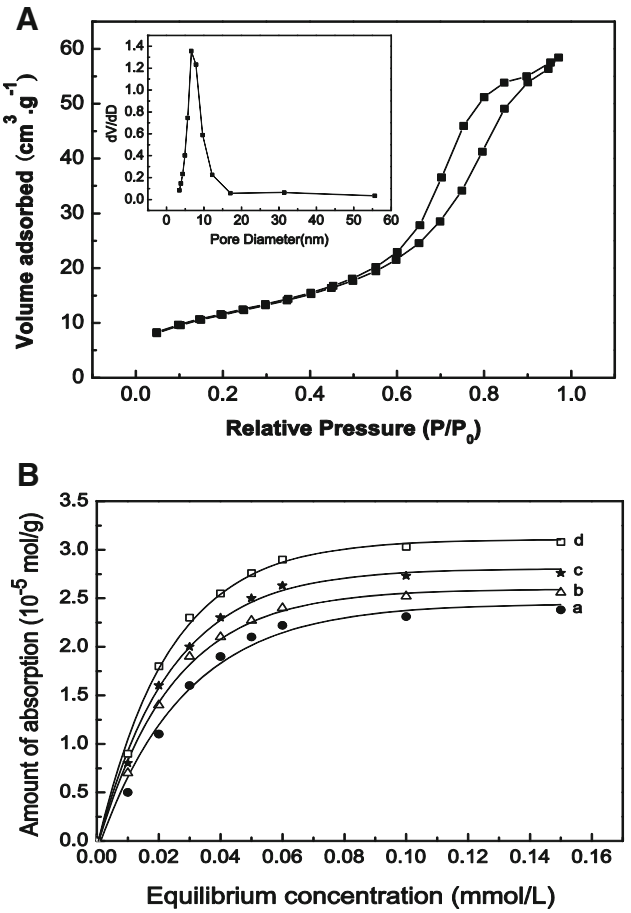

Figure 4. (**A**) Nitrogen adsorption–desorption isotherms and the corresponding pore size distribution (inset) for M-425. (**B**) Adsorption isotherms of orange II (a) M-625, (b) M-525, (c) M-470 and (d) M-425.

exhibits the highest photocatalytic activity among the samples (figure 7d). Removal efficiency of total organic carbon of orange II in the M-425/H_2O_2 system was analysed (shown in supporting information figure S2). The mineralization efficiency of orange II is slightly lower than the DE. It should be attributed that partial oxidation species were used to destroy the structure of pollutants to form small-molecule intermediates instead of complete oxidation to CO_2 and water. And most of the orange II can be mineralized in the M-425/H_2O_2 system.

The changes in the UV–Vis spectra with the reaction time during the photodegradation of orange II in the M-425/H_2O_2 system under the best degradation conditions are depicted in figure 8. The main absorption band at 484 nm and other bands at 228 and 310 nm in the ultraviolet region are observed. The former band corresponds to the n-π^* transition of the azo form, whereas the latter ones are attributed to the π^*–π^* transition of the benzoic and naphthalene rings, respectively [3]. These three absorption peaks gradually decrease and nearly disappear with further reaction, which indicates the destruction of the N=N bond and aromatic rings of orange II [29,30].

Table 1. SSA, TPV of different Fe_3O_4 samples and adsorption parameters of orange II on M-625, M-525, M-470 and M-425.

Samples	SSA	TPV	$\Gamma_{max} \times 10^{-5}$	$K_\alpha \times 10^4$	R^2
M-625	158.9	0.18	2.37	2.29	0.995
M-525	170.3	0.19	2.55	2.51	0.997
M-470	180.7	0.21	2.75	2.69	0.998
M-425	191.2	0.22	3.07	3.08	0.996

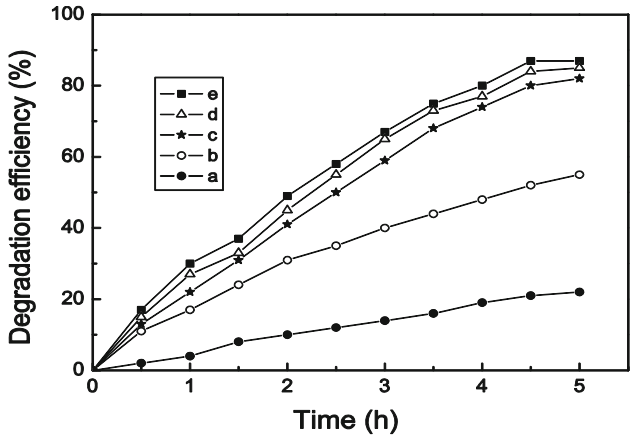

Figure 5. Effects of concentration of H_2O_2 on the photodegradation of orange II in the M-425 system: (a) 0 mM, (b) 1 mM, (c) 2 mM, (d) 3 mM and (e) 4 mM.

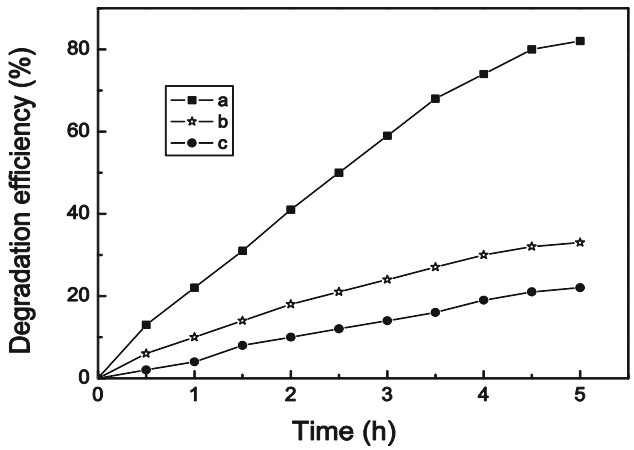

Figure 6. DE of orange II in the M-425 system under different conditions: (a) 2 mM of H_2O_2, visible light irradiation; (b) 2 mM of H_2O_2, dark and (c) 0 mM of H_2O_2, visible light irradiation.

To evaluate the stability of the prepared Fe_3O_4, the catalytic performance of M-425 was tested in five subsequent oxidation cycles under identical conditions. After each experiment, the catalyst was separated from the treated solution by a magnetic separation method. The obtained results indicate that the M-425 photocatalyst can be reused effectively several times

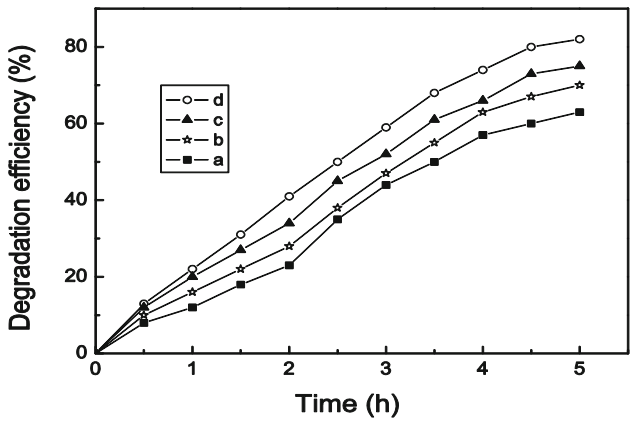

Figure 7. DE of orange II with reaction time in the presence of different Fe_3O_4 samples with 2.0 mM H_2O_2 under visible light irradiation at pH 3: (a) M-625, (b) M-525, (c) M-470 and (d) M-425.

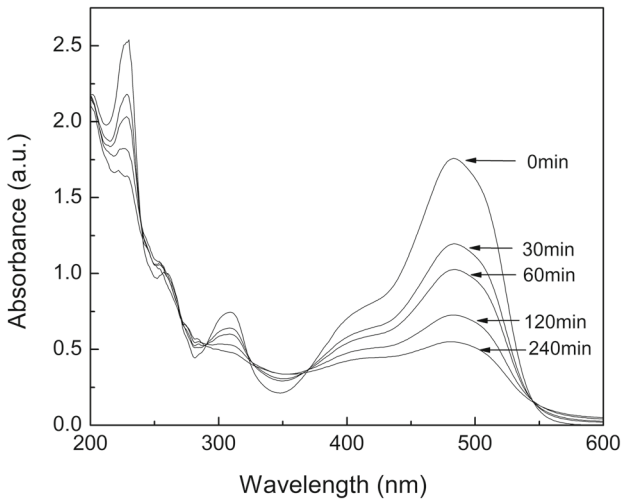

Figure 8. UV–Vis spectral changes of orange II in the M-425/H_2O_2 system.

without significant losses in activity (figure 9). After recycling M-425 five times, the DE of orange II ranges from 82 to 66%. This finding suggests that the photocatalytic activity of the M-425 catalyst did not degrade easily even after recycling.

To further analyse the reasons for the differences in photocatalytic degradation of samples, the UV–Vis absorption spectra of M-625, M-525, M-470 and M-425 were recorded (figure 10A). Obviously, with the decrease in the size of the samples, the Fe_3O_4 nanoparticles can cause an appropriate red shift. The band gap energy (E_g) was then calculated by using the formula $E_g = 1240/\lambda$, where λ is the cut-off wavelength [31,32]. The calculated E_g values of M-625, M-525, M-470 and M-425 are 1.82, 1.80, 1.69 and 1.54 eV, respectively. This renders the small-particle-sized Fe_3O_4 samples with better photocatalytic activity under visible light irradiation.

In addition, in the Fenton systems, H_2O_2 is catalytically decomposed into active $^{\bullet}OH$ radicals that initiate the chain

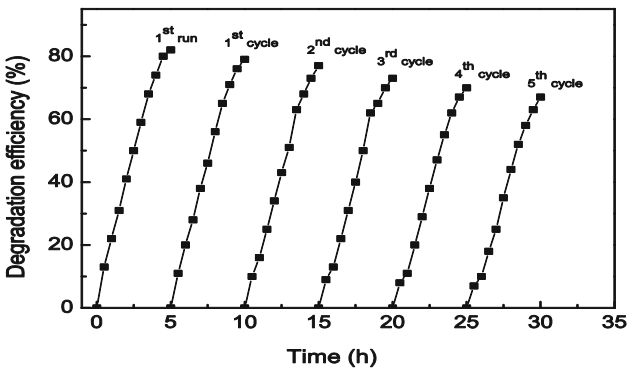

Figure 9. Stability of M-425 catalyst after subsequent reactions under identical conditions (2 mM of H_2O_2, visible light irradiation and pH 3).

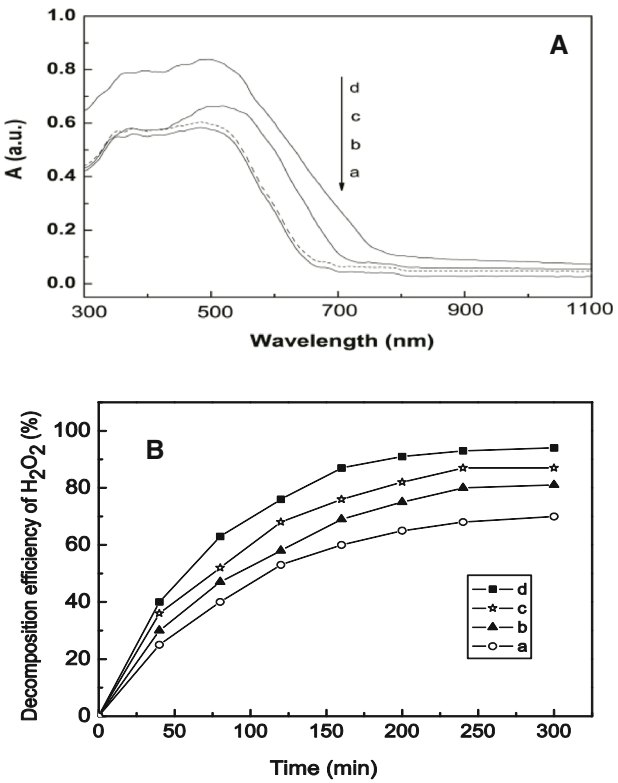

Figure 10. (**A**) UV–Vis absorption spectra of different Fe_3O_4 samples. (**B**) Decomposition efficiency of H_2O_2 in the presence of different Fe_3O_4 samples: (a) M-625, (b) M-525, (c) M-470 and (d) M-425.

reaction; thus, the decomposition rate of H_2O_2 plays a pivotal role in the process [33,34]. In our apparatus, the H_2O_2 concentrations were measured in different Fe_3O_4 systems with further reaction (figure 10B). The DE of H_2O_2 enhances gradually with the decrease in the size of the Fe_3O_4 nanoparticles, which means the small-particle-sized Fe_3O_4 samples demonstrate high activity and favours the decomposition of H_2O_2 (figure 10B-d).

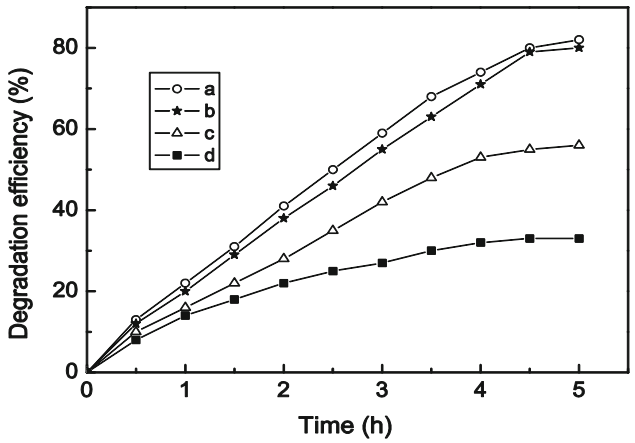

Figure 11. Reactive species trapping experiments in the M-425/H_2O_2 system: (a) M-425/H_2O_2, (b) M-425/H_2O_2 + BZQ, (c) M-425/H_2O_2 + Na_2-EDTA and (d) M-425/H_2O_2 + *tert*-butanol.

During the photoreaction, a small amount of Fe_3O_4 samples could be photodissolved in the solution to produce Fe(III) and Fe(II) ions, then the dissolved Fe(III) species could be partially photoreduced to Fe(II) species [35]. In our case, the amount of total dissolved iron increased during the photodegradation (supporting information figure S3). The concentrations of the dissolved iron increase with the decrease in the size of samples. The dissolved iron can exhibit the photodegradation of orange II through a homogeneous photo-Fenton reaction [36]. Furthermore, the small-particle-sized Fe_3O_4 with a high-adsorption ability is expected to enhance the photodegradation of dyes [37]. Fe(III)–OH and Fe(II)–OH can combine with H_2O_2 to form $OH^\bullet$ through the heterogeneous photo-Fenton reaction (equations (2 and 3)) [38]. In addition, the electrons and holes are photogenerated on the surface of Fe_3O_4 under light irradiation (equation (4)). O_2 in the solution can combine with the e^- (aq.) to form $O_2^{-\bullet}$:

$$\text{Fe(III)–OH} + H_2O_2 + h\nu \rightarrow \text{Fe(II)–OH} + HO_2^\bullet \quad (2)$$

$$\text{Fe(II)–OH} + H_2O_2 + h\nu \rightarrow \text{Fe(III)–OH} + OH^\bullet + OH^- \quad (3)$$

$$\text{Fe(III)–OH} + h\nu \rightarrow e_{cb}^- + h_{vb}^+ \quad (4)$$

In our case, radical-trapping experiments were performed in the M-425/H_2O_2 systems by using three different chemicals (BZQ, Na_2-EDTA and *tert*-butanol are the scavengers of $O_2^{-\bullet}$, h_{vb}^+ and $OH^\bullet$, respectively) [39–41]. Figure 11 illustrates that the presence of Na_2-EDTA results in the decrease of the DE of M-425 (figure 11c), and the addition of *tert*-butanol causes a rapid decrease in the photocatalytic activity (from 82 to 33% at 5 h) (figure 11d). Moreover, the employment of BZQ in the system shows a negligible effect on its excellent photocatalytic activity (figure 11b). These results imply that the $OH^\bullet$ radicals and holes largely contribute to the highly efficient photocatalytic performance. The $^\bullet$OH radicals are mainly responsible for the degradation of orange II.

Table 2. DE of orange II at 5 h in variable-sized Fe_3O_4 systems with and without *tert*-butanol.

Samples	M-625	M-525	M-470	M-425
DE of orange II without *tert*-butanol (%)	63	70	75	82
DE of orange II with *tert*-butanol (%)	28	30	32	33

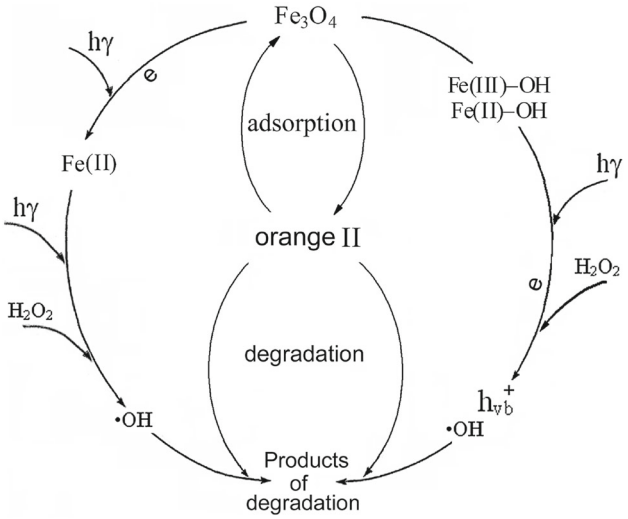

Figure 12. Proposed scheme for orange II photocatalytic degradation in the Fe_3O_4/H_2O_2 system.

Additionally, the DEs of orange II in different Fe_3O_4 systems (the best degradation condition) in the presence or absence of *tert*-butanol ($^\bullet$OH scavenger) were analysed. The DEs of orange II at 5 h in variable-sized Fe_3O_4 systems with and without *tert*-butanol are listed in table 2. The DEs of orange II decrease significantly in all the Fe_3O_4 systems when *tert*-butanol is added to the reaction system. In the M-425 system, the DE of orange II shows the greatest decrease, which indicates that the highest content of $^\bullet$OH radicals is produced in the M-425 system. The possible pathway for the photocatalytic degradation of orange II with the Fe_3O_4 photocatalyst is shown in figure 12.

4. Conclusions

Fe_3O_4 nanoparticles with variable sizes (9.9–29.1 nm) were obtained under light irradiation with various wavelengths at room temperature. With the decreasing wavelength of light irradiation, the particle sizes of the Fe_3O_4 nanocrystals

decreased gradually. With the decrease in the size of the Fe_3O_4 nanoparticles, the Fe_3O_4 samples exhibited a large surface area and high adsorption. Meanwhile, the as-prepared Fe_3O_4 samples with small particle sizes caused an appropriate red shift of the spectra and favoured the decomposition of H_2O_2, which produced high-content $^{\bullet}OH$ radicals by photo-Fenton reaction, leading to high-photocatalytic degradation of orange II.

Acknowledgement

This work was supported by a Grant from the Natural Science Foundation of China (21477032 and 21277040).

References

[1] Devi L and Kavitha R 2013 *Appl. Catal.: B Environ.* **141** 559
[2] Zhang H, Li Y, Zhong X and Ran X 2011 *Water Sci. Technol.* **63** 1373
[3] Luo M, Lv L, Deng G, Yao W, Ruan Y, Li X *et al* 2014 *Catal. A: General.* **469** 198
[4] Duan L, Sun B, Wei M, Luo S, Pan F, Xu A *et al* 2015 *J. Hazard. Mater.* **2285** 356
[5] Usman M, Faure P, Ruby C and Hanna K 2012 *Appl. Catal. B: Environ.* **117** 10
[6] Hanna K, Kone T and Medjahdi G 2008 *Catal. Commun.* **9** 955
[7] Xue X, Hanna K, Abdelmoula M and Deng N 2009 *Appl. Catal. B: Environ.* **89** 432
[8] Hou L, Zhang Q, Jérôme F, Duprez D, Zhang H and Royer S 2014 *Appl. Catal. B: Environ.* **144** 739
[9] Deng J H, Wen X H and Wang Q N 2012 *Mater. Res. Bull.* **47** 3369
[10] Zhang S X, Zhao X L, Niu H Y, Shi Y L, Cai Y Q and Jiang G B 2009 *J. Hazard. Mater.* **167** 560
[11] Sun S P and Lemley A T 2011 *J. Mol. Catal. A: Chem.* **349** 71
[12] Zhang J B, Zhuang J, Gao L Z, Zhang Y, Gu N, Feng J *et al* 2008 *Chemosphere* **73** 1524
[13] Xue X F, Hanna K and Deng N S 2009 *J. Hazard. Mater.* **166** 407
[14] Rusevova K, Kopinke F D and Georgi A 2012 *J. Hazard. Mater.* **241–242** 433
[15] Wang N, Zhu L H, Wang D L, Wang M Q, Lin Z F and Tang H Q 2010 *Ultrason. Sonochem.* **17** 526
[16] Rakhshaee R 2014 *Powder Technol.* **254** 494
[17] Chang Q, Zhu L, Luo Z, Lei M, Zhang S and Tang H 2011 *Ultrason. Sonochem.* **18** 553
[18] Yang T, Shen C, Li Z, Zhang H, Xiao C, Chen S *et al* 2005 *J. Phys. Chem. B* **109** 23233
[19] Si S, Wang C X, Yu D, Peng Q and Li Y 2005 *Cryst. Growth Des.* **5** 391
[20] Kulkarni S A, Sawadh P S, Palei P K and Kokate K K 2014 *Ceram. Int.* **40** 1945
[21] Chen R, Song G and Wei Y 2010 *J. Phys. Chem. C* **114** 13409
[22] Liu H, Wei Y and Sun Y 2005 *J. Mol. Catal. A: Chem.* **226** 135
[23] Pablo S P, Victor A O, Flavio L S and Versiane A L 2010 *Biochem. Eng. J.* **51** 194
[24] Wang X, Liu C, Li X, Li F and Zhou S 2008 *J. Hazard. Mater.* **153** 426
[25] Chen R, Zhao S, Liu H, Song X and Wei Y 2015 *J. Photochem. Photobiol. A* **312** 73
[26] Belin T, Guigue-Millot N, Caillot T, Aymes D and Niepce J C 2002 *J. Solid State Chem.* **163** 459
[27] Bao S, Tang L, Li K, Ning P, Peng J, Guo H *et al* 2016 *J. Colloid Interface Sci.* **462** 235
[28] Li Z, Meng G, Chen R and Song X 2015 *RSC Adv.* **5** 88787
[29] Mu Y, Yu H Q, Zheng J C and Zhang S J 2004 *J. Photochem. Photobiol. A* **163** 311
[30] Deng J H, Jiang J Y, Zhang Y Y, Lin X P, Du C M and Xiong Y 2008 *Appl. Catal. B: Environ.* **84** 468
[31] Liu R, Ji Z, Wang J and Zhang J 2018 *Microporous Mesoporous Mater.* **266** 268
[32] Kumar S G and Rao K S R K 2015 *RSC Adv.* **5** 3306
[33] Filip J, Zboril R, Schneeweiss O, Zeman J, Cernik M, Kvapil P *et al* 2007 *Environ. Sci. Technol.* **41** 4367
[34] Ma Y, Meng S, Qin M, Liu H and Wei Y 2012 *J. Phys. Chem. Solids* **73** 30
[35] Lei J, Liu C S, Li F B, Li X M, Zhou S G, Liu T X *et al* 2006 *J. Hazard. Mater.* **137** 1016
[36] Fan X, Hao H, Shen X, Chen F and Zhang J 2011 *J. Hazard. Mater.* **190** 493
[37] Wang Y, Zhao Y, Ma Y, Liu H and Wei Y 2010 *J. Mol. Catal. A: Chem.* **325** 79
[38] Wu J J, Muruganandham M, Yang J S and Lin S S 2006 *Catal. Commun.* **7** 901
[39] Yang X, Cui H, Li Y, Qin J, Zhang R and Tang H 2013 *ACS Catal.* **3** 363
[40] Yang X, Qin J, Jiang Y, Li R, Li Y and Tang H 2014 *RSC Adv.* **4** 18627
[41] Cui H, Yang X, Gao Q, Liu H, Li Y, Tang H *et al* 2013 *Mater. Lett.* **93** 28